Biomimetic cell structures: Probing Induced pH-Feedback Loops and pH Self-Monitoring in Cytosol Using Binary Enzyme-loaded Polymersomes in Proteinosome

Kehu Zhang,[a,b] Silvia Moreno,*[a] Xueyi Wang,[c] Yang Zhou,[a,b] Susanne Boye,[a] Dagmar Voigt,[d] Brigitte Voit,[a,b] Dietmar Appelhans*[a]

[a]Leibniz-Institut für Polymerforschung Dresden e.V.; Hohe Straße 6, Dresden 01069, Germany; applhans@ipfdd.de; moreno@ipfdd.de

[b]Chair of Organic Chemistry of Polymers; Technische Universität Dresden; Dresden 01062, Germany

[c]Affiliated Dongguan Hospital, Southern Medical University, Dongguan 523059, P. R. China

Abstract

Structures and functions of eukaryotic cells with an outer permeable membrane, motility, a cytoskeleton, biomolecules diffusion, and functional organelles can be imitated by a multi-compartmentalized and large-sized protocell containing various synthetic organelles. Herein, two kinds of artificial organelles with stimuli-trigged regulation ability, glucose oxidase-(GOx)-loaded pH-responsive polymersomes A (GOx-Psomes A) and urease-loaded pH-responsive polymersomes B (Urease-Psomes B) for probing biomimetic pH homeostasis, and a pH-sensor (Dextran-FITC) are encapsulated into proteinosomes by Pickering emulsion method. Thus, the polymersomes-in-proteinosome system is realized. Alternating input-regulation of fuels (glucose or urea) outside the protocell penetrates the membrane of proteinosomes and enters into GOx-Psomes A and Urease-Psomes B to produce chemical\biological signals (gluconic acid or ammonia) resulting in pH-feedback loops (pH jump and pH drop). This will counteract the catalytic “switch on” or “switch off” of enzyme-loaded Psomes A and B owing to their different pH-responsive membranes. Thus, the Dextran-FITC promotes a controlled cytosolic spatial organization and the detection of slight pH fluctuations in the lumen of protocells. Overall, this approach shows heterogeneous polymersome-in-proteinosome architectures with sophisticated features such as induced input-regulated pH changes mediated by negative/positive feedback in loops and cytosolic pH self-monitoring, requirements strictly needed in an advanced protocell design.

Introduction

The eukaryotic cell is not only one of the most basic life units in nature but also one of the most complex biological structures containing a cell membrane with recognition ability, a cytoskeleton, and several functional organelles (nucleus, lysosome, Golgi apparatus, mitochondria, etc.). Its complexity, hierarchical microstructures, and functions have attracted

strong attention and extensive research by scientists for understanding and imitating eukaryotic cells.[1-3] Inspired by cells, various large-sized giant vesicles (micron scale) with and without membranes[4-14] were realized to encapsulate synthetic organelles (secondary-size, nanoscale), such as micelles,[4] polymersomes,[9,10,15] liposomes,[6,16] coacervates[17-19] or dendrimersomes[20] to fabricate artificial multi-compartmentalized protocells. Moreover, cell functions such as division,[21,22] fusion,[23,24] endocytosis,[16,22] exocytosis,[25] and substance exchange and signal transmission between cell-cell,[26-29] cell-internal organelles,[4] or organelle-organelle,[15,16,30-32] have been mimicked by multi-compartmentalized structures.

Cells are biological units with pH homeostasis and self-regulation ability. They are capable of automatically adjusting the pH level to a pH equilibrium after the pH out-of-equilibrium state triggered by external stimulus such as temperature, biological or chemical fuels, or extracellular pH.[33-35] Consequently, synthetic organelles with pH stimuli-responsive properties in protocells have been previously established such as polymersomes-in-proteinosome (PsomesP),[9,10] coacervate-in-liposome,[36] coacervate-in-proteinosome,[17] even prototissues assembled by pH-responsive proteinosome[37]. However, all mentioned systems are far from simulating the pH self-regulation of equilibrium and non-equilibrium transitions in protocells.

Interestingly, the process of (counter-)trigger (H+/OH−) mediated by enzyme-catalyzed reactions composed of a binary of antagonistic enzymes from organisms, urease and glucose oxidase (GOx), and corresponding chemical fuels (urea and glucose), may be one of the best ways to mimic pH self-regulation of the cell. In the last decade, antagonistic GOx−glucose and urease−urea reaction causing opposite changes in pH within one system unified has been applied to various systems such as polymersomes, hydrogels, and multi-compartmentalized structures.[38-42] Mann and co-workers investigated an antagonistic chemical coupling in self-reconfigurable host-guest protocells by adding glucose and urea to achieve morphological and structural transformation of the mixing of proteinosome containing encapsulated GOx/urease and non-encapsulated fatty acid vesicles as pH increases or decreases.[39] Willner et al. reported a biocatalytic reversible control of responsive binary enzymes loaded hydrogel composed of GOx/urease for shape-memory, self-healing, and controlled release of insulin by suppling glucose and urea.[40]

Recently, our group demonstrated an artificial organelle system (AOS) based on photo-crosslinked GOx-loaded polymersomes A (GOx-Psomes A) and photo-crosslinked urease-loaded polymersomes B (Urease-Psomes B) with pH-responsive membranes to achieve reciprocating pH changes.[38] The glucose or urea inputs trigger a dynamic state of AOS for sequential changes in the catalytic activity of enzymes and pH drops and jumps, showing an

input-regulated pH-feedback loops (IRPFL).Therefore, the next step is to transfer the above concept to a multicompartmental artificial protocell for achieving spatiotemporal control of time-dependent cellular processes and pH regulation. The design and an adequate characterization of the structure and function of this artificial protocell under cytosolic-like conditions is a challenge and a crucial step toward intelligent biomimetic systems.

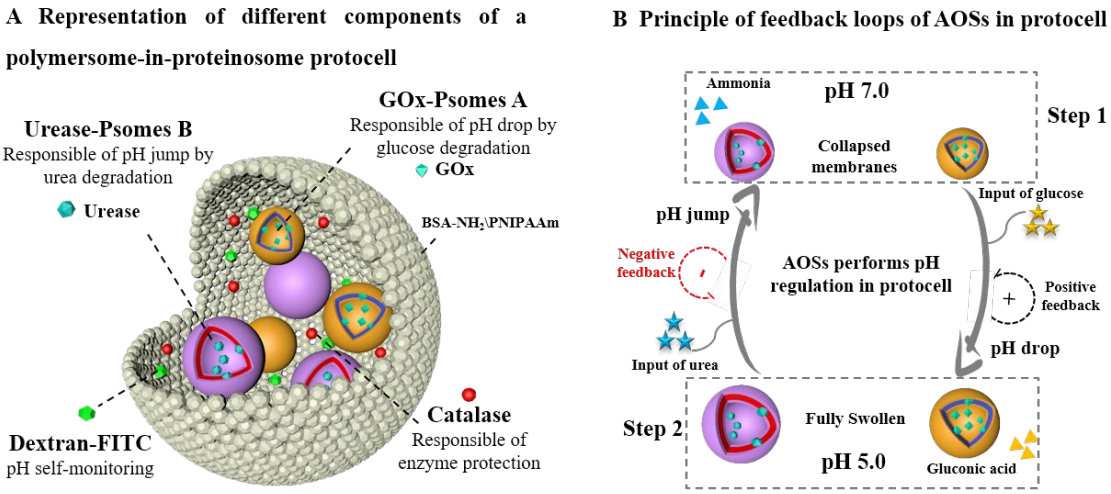

Scheme 1. A) Representation of a PsomesP protocell including AOSs (antagonistic GOx-Psomes A and Urease-Psomes B), catalase, and Dextran-FITC as pH sensor in proteinosomes. Catalase (CAT) responsible for the degradation of toxic H_2O_2 into ½ O_2 and H_2O in the multicompartmental environment of PsomesP protocell. B) Schematic overview of the principle of enzymatic reactions induced feedback loops via the coupling of positive (pH drop and AOSs membrane swollen) and negative feedback (pH jump and AOSs membrane collapsed) by multiple inputs at different states (glucose and urea).

Hence, an artificial organelles-in-protocell system (AOPS) with heterogeneous multi-compartmentalized PsomesP structures, an IRPFL and cytosolic pH self-monitoring abilities was designed and constructed. For this aim, antagonistic GOx-Psomes A and Urease-Psomes B, catalase responsible for enzyme protection through a detoxifying step of H_2O_2 into ½ O_2 and H_2O, and Dextran-FITC as pH sensor, were encapsulated into proteinosome through Pickering emulsion method (Scheme 1A). The input of chemical and biological fuels (glucose or urea) takes place outside the protocells. Then, substrates diffuse to the inner part, and the products (chemical and biological metabolites: gluconic acid and ammonia) of GOx-Psomes A and Urease-Psomes B result in drop or jump of pH due to H^+ produced by ionization of gluconic acid and OH^- generated by protonation of ammonia. Glucose

input at pH 7 in AOPS (Step 1) generates gluconic acid under the catalysis of GOx, leading to pH drop and facilitating complete swelling of both Enzyme-Psomes and influx of substrate in a positive feedback loop (increase of enzymatic activity, Scheme 1B). Conversely, the urea input (Step 2) generates alkali under catalysis of urease, resulting in opposite process and coming back to the starting point in a negative feedback loop (reduction of enzymatic activity, Scheme 1B). The feedback pH changes will counter-trigger AOS in different states due to pH-responsive membranes. The pH-feedback loops (pH drop and jump cycles) and pH self-monitoring ability were clearly presented by sequential input-regulation of chemical and biological fuels at Step I and Step II in AOPS (Scheme 1B).

Results and discussion

Construction of artificial organelles: GOx-Psomes A and Urease-Psomes B

The pH-responsive and crosslinked Psomes have previously been used to incorporate active biomacromolecules, especially enzymes, to design artificial organelles. They are versatile, chemically and physically stable, membrane permeability for different bio(macro)molecules, and capable of regulating enzyme activity through the pH-sensitive membrane permeability,[9,10,38,43-52] such as crosslinking and permeabilizing of pH-responsive GOx/CAT-Psomes by S. Liu group[50]. The preparation process and characterization methods of artificial organelles GOx-Psomes A and Urease-Psomes B are based on our previous report,[38,43,47] at which the collapsed membrane state of pH-responsive Psomes does not allow the feeding of lumen-located enzyme in Psomes with any low-molecular weight substrate or intermediates (e.g. glucose or H_2O_2).[38,43,44,46,51]

To construct two kinds of Enzyme-Psomes with different pH-responsive membrane, amphiphilic block copolymers $mPEG_{45}$-*b*-P(DEAEMA-*co*-DMIBMA) (BCP-A) and $mPEG_{45}$-*b*-P(DPAEMA-*co*-DMIHMA) (BCP-B) were successfully synthesized by atom transfer radical polymerization (ATRP).[38,43,46,47] The synthesis, characterization and analysis of BCP-A and BCP-B, and Empty-Psomes self-assembled by the pH switch method as a reference are shown in Scheme S1 and S2. Fig. S2-S4, Fig. S7-S9 and Table S1†. GOx (0.2 mg mL^{-1}) and Urease (0.1 mg mL^{-1}) were loaded into Psomes A (1.0 mg mL^{-1}) and Psomes B (1.0 mg mL^{-1}), respectively, by *in-situ* loading method. Afterwards, the samples were UV light irradiated (90s for GOx-Psomes A and 180s for Urease-Psomes B) and purified by hollow fibre filtration (HFF) (Fig. 1A).[38,47] To calculate the encapsulation efficiency (EE) of enzymes and to monitor the HFF purification process, labelled enzymes were loaded (GOx-FITC and Urease-Alexa 350) (Fig. S17†). The EE of GOx-FITC (λ_{ex} = 495 nm and λ_{em} = 519 nm) and Urease-Alexa 350 (λ_{ex} = 350 nm and λ_{em} = 442 nm) were 13.6% and 23.5%, respectively, which were calculated by fluorescence intensity before and after purification by HFF. Vesicular structures of artificial organelles were observed by cryo-TEM under basic conditions (collapsed state of Psomes membrane, Fig. 1A). The average diameter and membrane thickness of GOx-Psomes A are 76.8 ± 6.0 nm and 18.3 ± 1.4 nm, respectively. In contrast, Urease-Psomes B feature

a larger size and membrane thickness, 112.5 ± 19.5 and 18.8 ± 2.6 nm. The Enzyme-Psomes show the same stability and robustness as the analogous Empty-Psomes, which were verified from the pH-dependent DLS study of repeatedly swelling-shrinking cycles between higher and lower pH levels (5 cycles). Thus, the hydrodynamic diameter of GOx-Psomes A at pH 5 and pH 8 (Fig. S16†) is 140 nm (swollen state at acid pH after amine protonation of the DEAEMA) and 85 nm, respectively. The hydrodynamic diameter of Urease-Psomes B at pH 4 and pH 7 is 190 nm (swollen state at acid pH after amine protonation of DPAEMA) and 125 nm. Overall this thoroughly indicates that both Enzyme-Psomes have excellent stability and reproducibility.

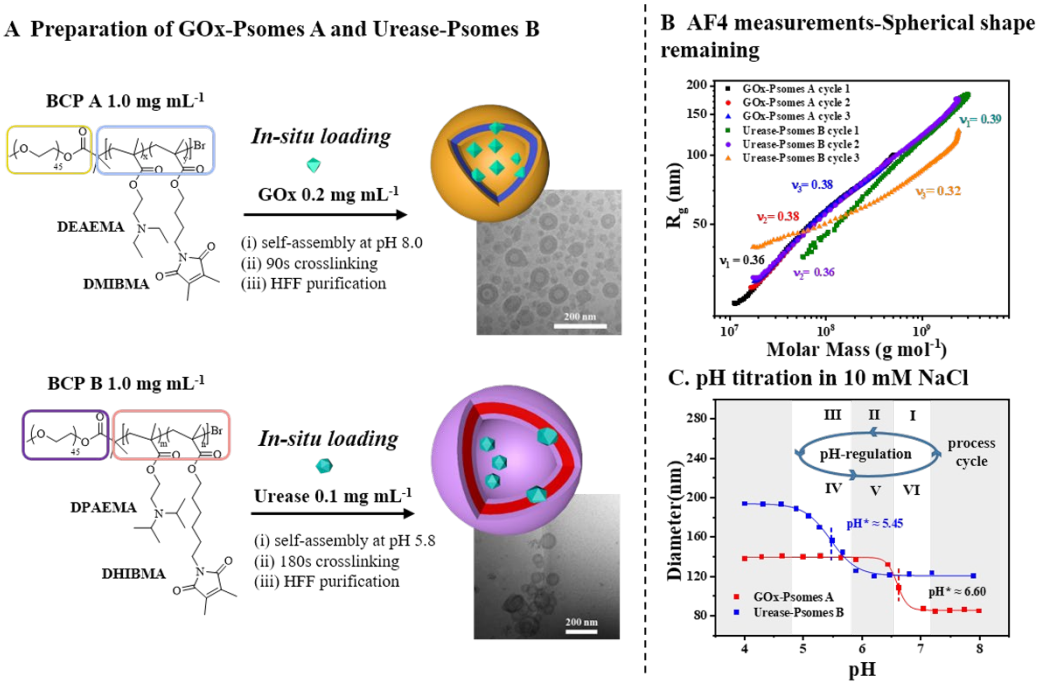

Fig. 1. Preparation and characterisation of GOx-Psomes A and Urease-Psomes B. A) Fabrication procedure for GOx-Psomes A and Urease-Psomes B with inserted cryo-TEM images, GOx-Psomes A with diameter Ø = 76.8 ± 6.0 nm and membrane thickness M = 18.3 ± 1.4 nm at pH 8 in 10 mM NaCl solution, Urease-Psomes B with diameter Ø = 121.6 ± 18.5 nm, membrane thickness M = 19.5 ± 2.4 nm at pH 7 in 10 mM NaCl solution. B) Conformation studies by AF4-LS for verifying spherical shape of GOx-Psomes A and Urease-Psomes B after HFF purification, scaling plots, R_g (circles) vs molar masses and three membrane swelling-shrinking cycles in 10 mM NaCl solution by manually adjusting pH determined. C) pH-dependent DLS data of GOx-Psomes A and Urease-Psomes B (Dot and squares for diameter obtained from DLS, − Logistic fit of the curve).

Asymmetrical flow-field flow fractionation with light scattering detection (AF4-LS) as a

powerful method to confirm molar mass, size, and conformational properties of Empty-Psomes and Enzyme-Psomes has been well established in our group.[9,10,38,44-48] Previous studies on GOx-Psomes A and Urease-Psomes B in PBS buffer at pH 7.0 and 5.0 by AF4-LS have been presented.[38] These results demonstrated that the scaling parameters *v* of GOx-Psomes A and Urease-Psomes B are relatively close to 0.33, implying Enzyme-Psomes with a regular spherical morphology at different conditions.[9,10,38,45-47] Fig. 1B shows the corresponding values of scaling parameter ν (0.32-0.39) of GOx-Psomes A and Urease-Psomes B in 10 mM NaCl solution within three swelling and shrinking cycles by manually adjusting pH using 0.1 M HCl or 0.1 M NaOH. It undoubtedly testifies that these two artificial organelles maintain their regular appearance of a vesicular structure after multiple pH-triggered swelling and de-swelling of the responsive membrane. The complete process can be well monitored by the light scattering (LS) and refractive index (RI) signals over elution time, but also by the calculation of the apparent density over molar mass of GOx-Psomes A and Urease-Psomes B (Fig. S20 and S21†). Summarizing the AF4-LS results, a high pH stability of both Enzyme-Psomes over several cycles in AOPS can be expected without losing the enclosed enzyme in the biomimetic pH-homeostasis.

Additionally, the *in-situ* loading, the purification method (HFF with shear-force driven separation process) and the recent results from this study support that the most enzymes are loaded in the lumen of Psomes as found before in previous studies.[38,46,51] The major difference between Psomes A and B is that they feature different pH* values (as half power of Psomes swelling) due to the different structure of the pH-responsive amine monomer, but pH* is also strongly influenced by the concentration of salts in the environment.[38,47] In Fig. 1C, pH 5.45 and pH 6.60 are shown respectively, for GOx-Psomes A and Urease-Psomes B, confirmed by pH-dependent DLS from pH 4 to pH 8 in 10 mM NaCl solution. The pH* values are slightly different compared with GOx-Psomes A and Urease-Psomes B in 1 mM PBS buffer previously reported due to salts concentration.[47] With this, the working principle of the two kinds of artificial organelles (Fig. 3) is defined by sequential and temporal control over pH for AOS in 10 mM NaCl solution, similar to what we reported earlier.[38] But an ordinary salt solution (10 mM NaCl solution) can more easily and clearly show the reciprocating pH changes in AOPS. To establish reciprocating pH changes in AOPS, the individual catalytic activity of both Enzyme-Psomes was first studied (Fig. S18†).

Construction of heterogeneous PsomesP as protocell

To carry out the study of multicompartmental AOPS based on PsomesP structures, the interfacial assembly at the water droplet/oil interface of a Pickering emulsion method was used to fabricate proteinosome by protein–polymer-conjugates such as bovine serum albumin (BSA) conjugated with poly(*N*-isopropylacrylamide) (PNIPAAm).[8-10] The synthesis, characterization and analysis of end-capped

mercaptothiazoline-activated PNIPAAm, cationized protein BSA-NH_2, and protein–polymer-conjugates BSA-NH_2/PNIPAAm are shown in Scheme S4, Fig. S10-14, and Tables S3 and S4†.

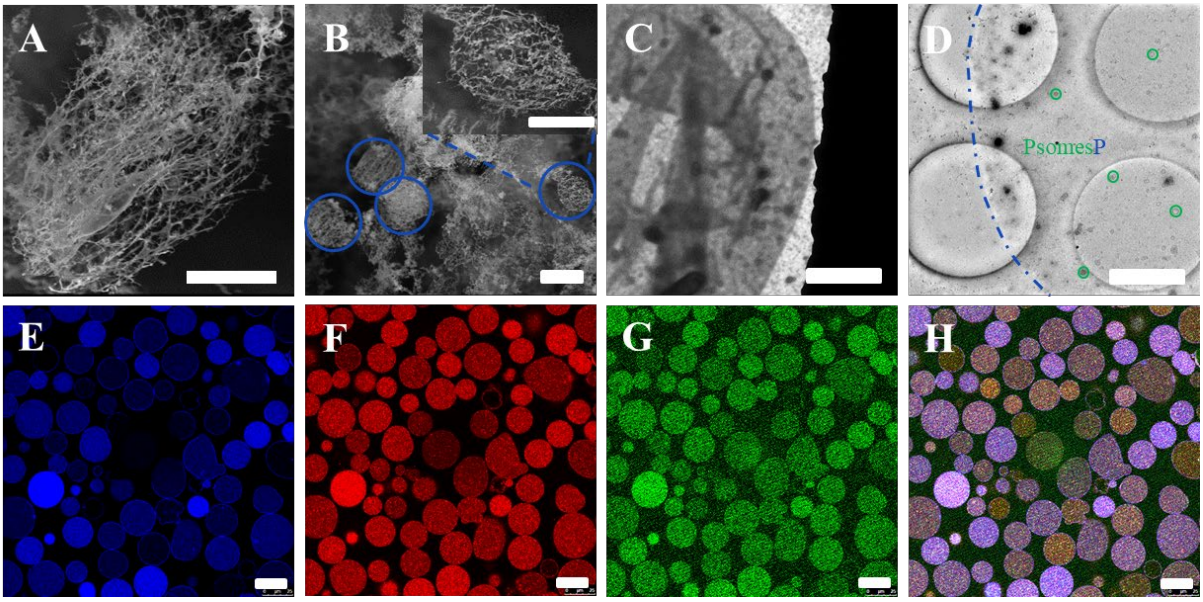

Fig. 2. A, B) Cryo-SEM images showing proteinosome loaded with GOx-Psomes A and Urease-Psomes B and Dextran-FITC in water (A: individual PsomesP structure, B: assembled PsomesP structures indicated by blue circles). The scale bar is 10 µm for image A, 20 µm for B, and 10 µm for inlet image of B, respectively. C) TEM image stained with uranyl acetate and D) cryo-TEM image of proteinosome loaded with GOx-Psomes A, Urease-Psomes B, and Dextran-FITC in water (Green circles indicate the presence of polymeric vesicles in PsomesP structure). The scale bar is 2 µm. CLSM images of proteinosome loaded with GOx-Psomes A-RhB and Urease-Psomes B-F in 10 mM NaCl solution, E) BSA/PNIPAAm labelled with Cy5 (λ_{ex} 630 nm), F) GOx-Psomes A-RhB containing BCPA-RhB (BCP-A copolymerized with RhB monomer, λ_{ex} 561 nm), G) Urease-Psomes B-F containing BCPB-F (BCP-B copolymerized with fluorescein monomer, λ_{ex} 488 nm), and superimposed E), F), and G) in H). The scale bar is 25 µm.

GOx-Psomes A-RhB (0.9 mg mL^{-1}), Urease-Psomes B-F (0.9 mg mL^{-1}), and catalase (0.17 mg mL^{-1}) were encapsulated in proteinosome by water-in-oil emulsification procedure using BSA-NH_2/PNIPAM (6.5 mg mL^{-1}). The EE of GOx-Psomes A-RhB (λ_{ex} = 555 nm and λ_{em} = 580 nm), Urease-Psomes B-F (λ_{ex} = 495 nm and λ_{em} = 519 nm) are 35.1% and 18.3%, respectively. The EE was calculated using the fluorescence intensity of the aqueous phase before and after purification (Fig. S22†). Cryo-SEM images of PsomesP show a network structure due to freezing and water sublimation process (Fig. 2A and 2B). The corresponding Enzyme-Psomes are not visualized because of their small size (approximately 100 nm).[9] Besides, the successful fabrication of PsomesP with multicompartmental structures was identified by TEM and cryo-TEM. Thus, the membrane of proteinosome and artificial organelles in its lumen can be intuitively observed as presented in Fig. 2C and 2D. The preparation of AOPS and subsequent phase

shifting (by centrifugation) can also remove unencapsulated Enzyme-Psomes. Artificial organelles (with typical polymeric vesicle structure) are shown in TEM and cryo-TEM images, while TEM image also shows membrane of proteinosome with a wrinkled structure after staining using uranyl acetate (Fig. 2C).[9,10]

Confocal laser scanning microscopy (CLSM) images can more clearly verify the heterogeneous multicompartmental structures of Enzyme-Psomes in proteinosome for AOPS. To achieve this, dye-labelled block copolymers, BCPA-RhB and BCPB-F (synthesis, characterization and analysis shown in Scheme S3, Fig. S5-6, and Tables S2†, were additionally used in the preparation process of GOx-Psomes A-RhB and Urease-Psomes B-F by mixing with BCP-A and BCP-B, respectively. As shown in Fig. 2E-2H, CLSM images suggest AOPS with an average size of 23.3 ± 5.6 μm, and two kinds of artificial organelles are available in the lumen of protocells. Thus, the colors, blue, red and green, represent BSA-NH_2/PNIPAAm-Cy5 (λ_{ex} = 630 nm), GOx-Psomes A-RhB (λ_{ex} = 561 nm) and Urease-Psomes B-F (λ_{ex} = 488 nm), respectively. Blue color in CLSM images (Fig. 2E and 2H) is also visible in the lumen of proteinosomes. From Fig. 2E-2G and Fig. S23† (cross-section of CLSM images of Fig. 2E-2G), the boundaries of the proteinosome can be clearly seen, and it can be clearly seen that almost all Psomes are in the area of Proteinosome. As a consequence, some protein–polymer conjugates, BSA-NH_2/PNIPAAm-Cy5, are also loaded as cargo together with GOx-Psomes A-RhB and Urease-Psomes B-F inside proteinosomes, leading to the same changes as observed for Empty-Proteinsome with increasing concentration of protein-polymer conjugates, BSA-NH_2/PNIPAAm-RhB (Fig. S15†). It is difficult to realize that all protein-polymer conjugates can be dispersed at the oil-water interface as a constituent unit of proteinosomes, since BSA-NH_2/PNIPAAm-Cy5 is also soluble in the water phase. Moreover, the complexity and incompleteness of the emulsification process are also influenced by the presence of high concentrations of Enzyme-Psomes and other components. In the same way, concentrations of artificial organelles vary in proteinosomes (Fig. 2F-2G). Counting the number of AOSs is a very tough challenge for AOPS protocell, since the characterization methods in this aspect have limitations. For CLSM, Psomes below 200 nm are very difficult to observe, and only dots are detected. And, it is hard to get enough TEM pictures with highly differentiated of PsomesP, as they are very large, while smaller Psomes are inside. Due to those limitations, no research paper obviously reported the number of secondary structures in the primary structure.[4,15-17,32]

Study of the IRPFL process in AOPS

The pH changes induced by enzymatic reactions (pH jump and pH drop) in an independent AOS based on GOx-Psomes A and Urease-Psomes B was previously studied by pH meter and optical

density measurements.[38] Similarly, the first experiments were carried out to optimize chemical and biological fuel concentrations to reach the desired pH using pH meter (Fig. 3A and 3B). Small chemical and biological fuels can penetrate into AOPS quickly and then react with artificial organelles inside, because of the molecular weight cut-off (≤ 70 kDa) of the proteinosome membrane.[9,10] In order to be able to show clearly the different states of the two Enzyme-Psomes (divided into six stages I–VI in Fig. 1C), the working pH range is set from 5.0 to 7.0). Different concentrations of substrate glucose (0.36, 0.54, 0.72 and 0.90 mg mL^{-1}) were added to AOPS at pH 7.0. Fig. 3A shows 0.54 mg mL^{-1} as the optimal concentration. The locally generated gluconic acid leads to pH decrease, permeable pH-sensitive membranes of AOS, and enhanced glucose influx in a positive feedback loop, which is very similar to that reported by S. Liu group[50]. After pH drop to 5.0 by adding glucose ($C_{glucose}$ =0.54 mg mL^{-1}), a pH jump of AOPS is observed by adding different concentrations of urea (0.06, 0.18, 0.30 and 0.42 mg mL^{-1}) (Fig. 3B), being 0.06 mg mL^{-1} the optimal concentration. Urease converts urea into ammonia, leading to pH increase and less permeable membranes of AOS, which is considered a negative feedback. The pH change in solution detected by pH meter also proves that both fuels, glucose and urea, can diffuse into the PsomesP structure. The heterogeneous Enzyme-Psomes population was assumed as homogeneous system in total due to the diffusion effect of enzymatic reaction product between all PsomesP structures. The substrates are consumed in the lumen of proteinosomes and the products diffuse out and move to different proteinosomes.

The input-regulated alternating pH change in the AOPS can be clearly divided into six stages I–VI as described in Fig. 3C (stages I-VI are the same as identified for different membrane states of Enzyme-Psomes in Figure 1C) and the schematic image in the middle of Fig. 3. Stage I: adding glucose at pH 7.0, the membrane of AOS, GOx-Psomes A, starts swelling due to its pH* is pH 6.60 in 10 mM NaCl solution, and another AOS, Urease-Psomes B, is in a collapsed state (pH 7.0−6.5); Stage II: the pH of AOPS continues to decrease, but GOx-Psomes A reach their fully opened state and remain fully opened, and Urease-Psomes B remain collapsed (pH 6.5−5.9); Stage III: GOx-Psomes A are still in a fully opened state, while Urease-Psomes B are in swelling state because its pH* is pH 5.45 in 10 mM NaCl solution (pH 5.9−5.0). Stage I-III are in positive feedback loop. Stage IV: when pH drops to 5.0, urea is added to AOPS and it can quickly diffuse through the membranes of the protocell. Urease-Psomes B are responsible for a rapid rise in pH, while GOx-Psomes A maintain completely opened and Urease-Psomes B are in shrinking state (pH 5.0−5.9); Stage V: when the pH of AOPS continues to increase, GOx-Psomes A are fully opened and Urease-Psomes B are in collapsed state (pH 5.9−6.5); Stage VI: GOx-Psomes A are shrunken to the fully closed state and Urease-Psomes B are still in collapsed state (pH

6.5−7.0). Stage IV-VI are in negative feedback loop.

The AOSs have a similar size drop as a function of pH change once these are encapsulated in the protocell, which can be concluded that each Enzyme-Psomes system undergoes different state transitions due to the pH changes. In Fig. 3C, the pH drop and jump cycle can be clearly divided into six stages I−VI according to the state (collapsed or swelling state, the Scheme in the middle of Fig. 3) of GOx-Psomes A and Urease-Psomes B, which is also verified by the results of the pH change cycle of AOPS in 10 mM NaCl solution against time after adding glucose at pH 7.0 and adding urea when the pH reaches near 5.0 (Fig. 3C and 3D). Especially in Fig. 3C, the different states of AOSs in protocell can also be clearly seen (six stages I−VI) as defined in Fig. 1C. In addition, two 'pH step' were also found since the protonation\deprotonation process of tertiary amino groups of DEAMA and DPAEMA at both pH values, and both Psomes membranes act as buffer, leading to decelerated pH changes (Fig. 3C; blue dots and red dots). These two 'pH steps' correspond to the pH* of GOx-Psomes A and Urease-Psomes B (pH 6.60 and pH 5.45 are shown in Fig. 1C, respectively).

Further aspects of the AOPS (Fig. 3C) are explained to clarify the mechanism of the IRPFL in the cytosol of PsomesP protocells. At the starting point pH 7, pH decreases slowly after adding glucose, although glucose concentration is at the highest level. This change in pH is caused by the fully closed membrane of AOS, GOx-Psomes A (Fig. 1C). Few GOx is located at the membrane's outer surface produce first protons to induce membrane protonation over time for switching on GOx activity located inside of Psomes at decreasing pH values. With the decrease of pH up to 5, the substrate glucose is almost consumed by GOx located on the inner surface of the membrane and lumen, as the membrane of GOx-Psomes A is completely swollen at pH ≤ 6.[46,51] After input of urea at negative feedback loop, the pH quickly jump to 7 from pH 5.0 since the Psomes membrane is in a fully open state and the urea can be converted by enzymes which are located as minor component in the membrane, but as major component in the lumen of Psomes. In a former study one experiment for the collapsed state of Urease-Psomes B was carried out by adding urea at pH 6.0 (Fig. S25), where Urease-Psomes B are in nearly the closed state. As a consequence, the pH starts to increase after 20 min and reaches pH 6.5 within a longer period than adding urea at pH 5.0.[38] This also implies for our recent study that the presence of some urease is in the membrane of Psomes B and the catalytic activity of most urease in lumen is restricted by the collapsed membrane.

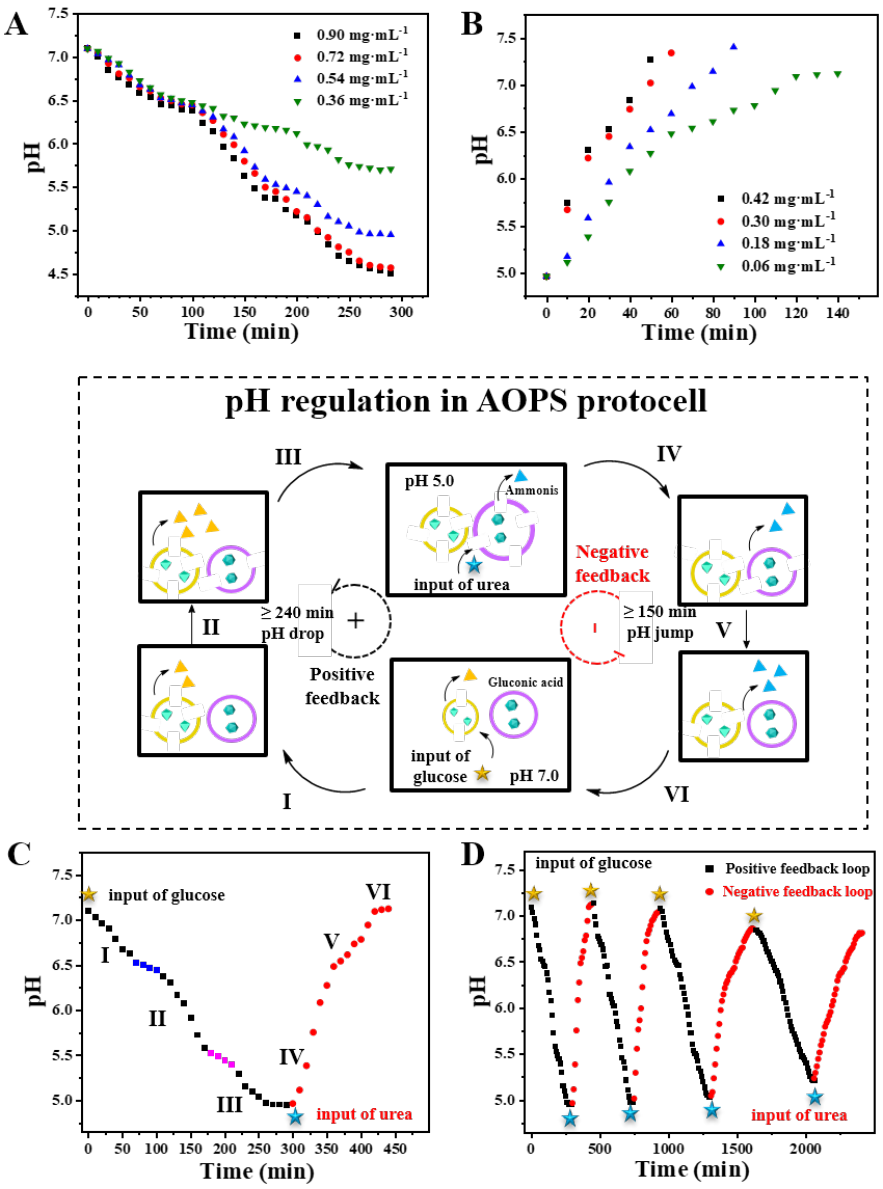

Fig. 3. A) pH change of AOPS protocell in 10 mM NaCl solution at pH 7.0 after adding different concentrations of glucose. B) pH change of AOPS in 10 mM NaCl solution after adding different concentrations of urea after pH reached pH 5.0. C) One pH change cycle of AOPS in 10 mM NaCl solution against time after adding 0.54 mg mL^{-1} of glucose at pH 7.0 and adding 0.06 mg mL^{-1} of urea when the pH reaches near 5.0. D) Reversible pH change cycles of AOPS in 10 mM NaCl solution against time after adding 0.54 mg mL^{-1} of glucose at pH 7.0 and adding 0.06 mg mL^{-1} of urea when the pH reaches near 5.0. Fig. in the middle: Schematic overview of IRPFL process in AOPS by the mixing of GOx-Psomes A and Urease-Psomes B as artificial organelles with pH-responsive membranes.[38] Statistics: First cycle of pH drop and jump for AOPS in Fig. 3C was carried out at least in quintuplicate each from different batches and reversible pH change cycles of AOPS in 10 mM NaCl solution (Fig. 3D) was carried out in quadruple (Fig. S28). Starting pH-dependency combined with fuel concentration on the first cycle of pH drop and jump for AOPS (Figure S26) was carried out in triplicate.

Overall, the process of substrate access to the enzymes is triggered by the swelling\shrinking state of Psomes (pH change) resulting from their pH responsive-membrane. In other words, the amount of enzymes involved in catalytic reaction changes as the permeability of the membrane changes. In order to show clearly the pH dependent enzyme activity of urease-Psome B and GOx-Psome A in AOPS, additional control experiments were carried out (Fig. S26†). In Fig. S26a, 0.54 mg mL^{-1} of glucose were added at pH 6.2 (Psomes A membrane is in open state) and at pH 7.2 (Psomes A membrane is in closed state) for studying the activity of the GOx-Psomes A at different states in AOPS. At pH 6.2, the rate of pH change is significantly faster than at pH 7.2, proving enzyme regulation by pH-sensitive membrane permeability in Psome A. In Fig. S26b, 0.06 mg mL^{-1} were added at pH 5 (Psomes B membrane is in open state) and at pH 6 (Psomes B membrane is in closed state) for studying the activity of the Urease-Psomes B at different states in AOPS. It was also found that the rate of pH change resulting by the urease-catalyzed reaction is greater when the membrane is in an open state. In both cases, enzyme activity can be observed even in the closed or impermeable states, but it must be considered that there is a small percentage of enzyme in the membrane which is still accessible by substrate at the collapsed membrane state. This is also supported by previous studies.[38,46]

In summary, pH drop is a positive feedback loop (the rate of glucose diffusion into the lumen is accelerated and AOS membrane goes from ‘off state’ to ‘on state’), while pH jump is a negative feedback loop (the rate of urea diffusion into the lumen is decelerated and AOS membranes goes from ‘on state’ to ‘off state’) (Fig. 3). Finally, there are many parameters (concentration of Enzyme-Psomes, enzyme loading efficiency, enzyme accessibility, fuel concentration, the rate of product ionization, etc.) to take into account for setting the rate of the pH drop/rise, but also the flexibility to adapt it to the desired application. Thus, the pH drop and jump can be completed in a short time and can complete multiple pH-feedback loops, which is the primary interest of our study.

For IRPFL, the dynamic and positive and negative feedback behavior in the AOPS is undoubtedly proven by multiple regulated inputs of chemical and biological fuels (glucose and urea) over four pH-feedback loops (Fig. 3D). It is found that the manual pH-feedback cycle time becomes longer with the increasing number of cycles. This is presumably caused by the increasing ion and metabolite concentration and their influence on the viscosity of intra- and extracellular matrix and diffusion properties of chemical and biological fuels. Thus, the enzymatic activity of AOPS inevitably slows down. However, it is positively noted in our present study of AOPS that even though the concentration of both Enzyme-Psomes (0.31 mg mL^{-1}, GOx-Psomes A and 0.16 mg mL^{-1} Urease-Psomes B) in AOPS is lower compared

to previous binary AOS (1.50 mg mL^{-1} GOx-Psomes A and 1.50 mg mL^{-1} Urease-Psomes B) in 1 mM PBS buffer[38], the enzymes are still active for IRPFL. Thus, the AOPS offers the potential of varying cyclic pH drops and jumps for other biomimetic intracellular requirements in protocells. Catalase with very high turnover numbers serves as an antioxidant defense system in AOPS protocell for long-term studies.[53]

Study on cytosolic pH self-monitoring for AOPS protocell

The pH meter can measure the change of pH outside proteinosomes via a contact manner, which indirectly reflects the pH change inside AOSP. Significantly, fluorescent molecules as pH sensors have been widely applied in artificial cells, cell imaging, drug carriers, and other systems.[54-56] The pH sensor can more conveniently and accurately detect the change of pH value *in-situ* and can be qualified for pH self-monitoring or self-imaging. Therefore, a sensor encapsulated in AOPS protocell can directly track and display the pH change in the lumen of the protocell.[9,10,17,36,57,58] Dextran, a neutral polysaccharide, has been widely used in pharmaceutical, biomedical, and food industries due to its high solubility, low viscosity, no gelation, and exceptional biocompatibility.[59,60] Nevertheless, Dextran-FITC with 150 kDa as a pH sensor was employed in AOPS to be suited for cytosolic pH self-monitoring.

The input of fuels (glucose or urea) in AOPS to produce gluconic acid or ammonia obviously result in a pH drop or a pH jump. Those processes can be immediately detected by pH sensors in cytoplasm (Fig. 4A). Fluorescence characteristics of Dextran-FITC, loaded in AOPS (EE 13%; Fig. S24a†) show the same trend with pH by manually adding acid and base. Therefore, Dextran-FITC can be used as pH sensor in AOPS (Fig. S24b†). The FITC on the dextran chain at pH 7.0 has a stronger fluorescence, while at pH 5.0 the neutral molecular state outlines a weaker fluorescence, since phenol (pK_a 6.4) and carboxylic acid (pK_a 5.0) groups of FITC are preferential in an ionized state in AOPS above pH 7.0 and in a deionized state below pH 5.0 (Fig. 4B).[61,62]

Here, the changes in the fluorescence intensity for AOPS (Fig. 4C and 4D) are attributed to the IRPFL state. For this, H^+ is produced by the ionization of gluconic acid and OH^- is generated by the protonation of ammonia. In the first cycle of pH jump and drop, fluorescence intensity and pH decrease with the catalytic time of GOx-Psomes A in presence of glucose, and increase with the catalytic time of Urease-Psomes B active after adding urea (Fig. 4C). This process can be reliably visualized by CLSM images (Fig. 4A and Fig. S27†), identifying different pH levels for the first cycle. As expected, fluorescence is higher at pH 7 than at pH 5. The pH self-monitoring function for Dextran-FITC as pH sensor in AOPS smoothly works within four cycles for IRPFL when adding continuously chemical and biological fuels glucose and urea at pH 7 and pH 5, respectively (Fig. 4D). In short, the fluorescence intensity decreases in positive feedback loop (pH drop) while increases in negative feedback loop (pH jump), which is also information

about feedback loops by regular signal input (glucose or urea). The transient time of fluorescence intensity of AOPS (equal to pH values in Fig. 4D) within four reversible cycles after repeated additions of fuels (adding glucose when pH reaches near 7.0 and adding urea when the pH reaches near 5.0) undoubtedly correlates with the transition time of pH for IRPFL (Fig. 3D). Each cycle of transient times by pH meter and pH sensor are summarized in Fig. S28†.

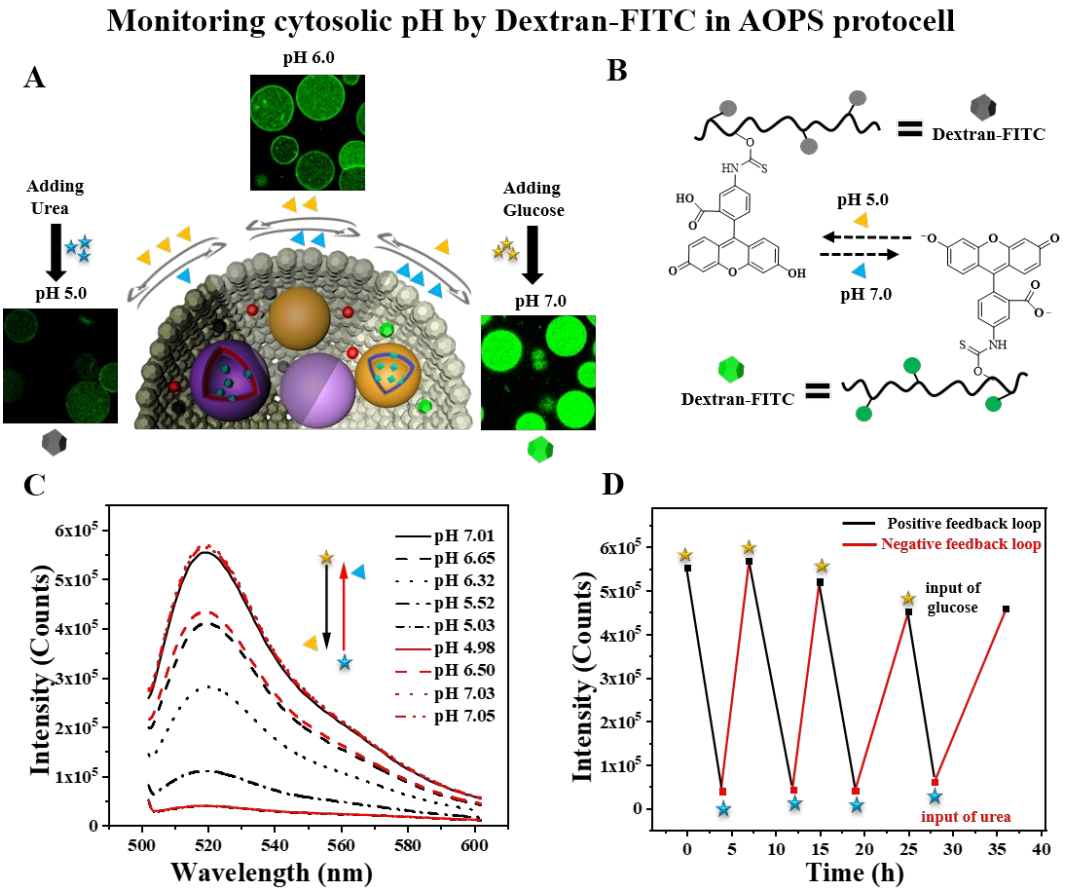

Fig. 4. A) Schematic representation of Dextran-FITC as pH sensor within AOPS and CLSM images (showing in Figuse S26) at pH 5.0, 6.0, and 7.0 in the first cycle of pH change after adding glucose and urea in 10 mM NaCl solution. B) Schematic representation of molecular structure changes of Dextran-FITC as pH sensor when pH change. C) Fluorescence spectra (λ_{ex} = 495 nm, λ_{em} = 500-605 nm) of the first cycle of pH change within AOPS after adding glucose and urea in 10 mM NaCl solution. D) Reversible pH change cycles of AOPS in 10 mM NaCl solution against time after adding glucose at pH 7.0 and adding urea when the pH reaches near 5.0 by fluorescence spectra (λ_{ex} = 495 nm, λ_{em} = 519 nm).

This heterogeneous AOPS with sophisticated features such as manually input-regulated pH

changes, and cytosolic pH self-monitoring is still far from eukaryotic cells with a smarter way of self-regulating intracellular pH. But the motivation of this AOPS was to establish biomimetic structures and functions to simulate pH homeostasis in a simpler way as eukaryotic cells can do through proton-pumps in combination with ATPase and/or other enzymatic cascade reactions to balance pH in various organelles and cytoplasm of cells.[33,34,63] With this approach of artificial protocells, we have shown a cooperative communication/exchange between protocells to tune the pH within the protocells driven by the signal transmission between cell-cell, cell-internal organelles, and/or organelle-organelle.

Conclusions

In summary, we demonstrated the successful fabrication of antagonistic artificial organelles in protocell, especially for the first time integrating a binary Enzyme-Psomes system with two different key characteristics of pH-responsiveness, catalase as H_2O_2-protector for involved enzymes and a polysaccharide, dextran as a pH sensor for local cytosolic pH self-monitoring. Induced pH-feedback loops of AOPS are achieved by enzyme-catalyzed reactions of GOx-loaded Psomes A and urease-loaded Psomes B with different pH-responsive membrane characteristics, leading to sequential and temporal control over their membrane permeability of each AOS. pH change loops (pH drop and jump cycles) are shown through a direct method (pH meter), an indirect method (pH sensor as pH-sensitive fluorescent dye), and reversibly stable spherical shapes verified by AF4-LS. Undoubtedly, the reversibility of pH changes and self-monitoring in AOPS protocell are smoothly realized by alternating regulated inputs of chemical and biological fuels (glucose and urea) at lowest and highest points of pH loops. Our smart AOPS protocell with a hierarchically multi-compartmentalized platform is one of the closest cases of artificial cells to mimic pH self-regulation of eukaryotic cells with pH homeostasis ability. This artificial protocell with high potential in systems biology may open new ways for advancing eukaryotic cell mimicry with various stimuli-responsive artificial organelles.

Data Availability Statements

Data are available upon request from the authors besides supplementary material in ESI.

Author Contributions

K.Z. carried out the majority experiments and the data analysis, wrote the major part of the original draft; S.M. designed and discussed the experiments and data analysis, manuscript revision. X.W. designed and discussed the experiments and data analysis; Y.Z. carried out part of experiments for the synthesis of BCP and Proteinosomes; S.B carried out experiments and analyzed AF4 measurements,

manuscript revision; D.V. carried out Cryo-SEM measurements, manuscript revision; B.V. project administration, manuscript revision; D.A project administration, first idea, supervision, writing and revision.

Conflicts of interest

There are no conflicts to declare.

Acknowledgements

K. Zhang are grateful for a scholarship under the Chinese government award by the China Scholarship Council (CSC). The authors thank Ms. Christina Harnisch for carrying out GPC (IPF Dresden), Dr. Petr Formanek for cryo-TEM study (IPF Dresden) and Dr. Martin Geisler for MALDI-TOF MS characterization (IPF Dresden). The Chair of Botany (C. Neinhuis) at the faculty of Biology of TU Dresden, Germany, is acknowledged for providing equipment and access to cryo-SEM.

References

1 J. W. Szostak, D. P. Bartel and P. L. Luisi, *Nature*, 2001, **409**, 387–390.

2 G. Pasparakis, N. Krasnogor, L. Cronin, B. G. Davis and C. Alexander, *Chem. Soc. Rev.*, 2010, **39**, 286–300.

3 P. R. LeDuc, M. S. Wong, P. M. Ferreira, R. E. Groff, K. Haslinger, M. P. Koonce, W. Y. Lee, J. C. Love, J. A. McCammon, N. A. Monteiro-Riviere, V. M. Rotello, G. W. Rubloff, R. Westervelt and M. Yoda, *Nat. Nanotechnol.*, 2007, **2**, 3–7.

4 S. Thamboo, A. Najer, A. Belluati, C. von Planta, D. Wu, I. Craciun, W. Meier and C. G. Palivan, *Adv. Funct. Mater.*, 2019, **29**, 1904267.

5 O. Kreft, A. G. Skirtach, G. B. Sukhorukov and H. Möehwald, *Adv. Mater.*, 2007, **19**, 3142–3145.

6 N.-N. Deng, M. Yelleswarapu, L. Zheng and W. T. S. Huck, *J. Am. Chem. Soc.*, 2017, **139**, 587–590.

7 M. Weiss, J. P. Frohnmayer, L. T. Benk, B. Haller, J.-W. Janiesch, T. Heitkamp, M. Börsch, R. B. Lira, R. Dimova, R. Lipowsky, E. Bodenschatz, J.-C. Baret, T. Vidakovic-Koch, K. Sundmacher, I. Platzman and J. P. Spatz, *Nat. Mater.*, 2018, **17**, 89–96.

8 X. Huang, M. Li, D. C. Green, D. S. Williams, A. J. Patil and S. Mann, *Nat. Commun.*, 2013, **4**,

2239.

9 P. Wen, X. Wang, S. Moreno, S. Boye, D. Voigt, B. Voit, X. Huang and D. Appelhans, *Small*, 2021, **17**, 2005749.

10 D. Wang, S. Moreno, S. Boye, B. Voit and D. Appelhans, *Chem. Commun.*, 2021, **57**, 8019–8022.

11 M. Li, R. L. Harbron, J. V. M. Weaver, B. P. Binks and S. Mann, *Nat. Chem.*, 2013, **5**, 529–536.

12 L. Rodríguez-Arco, M. Li and S. Mann, *Nat. Mater.*, 2017, **16**, 857–863.

13 M. J. Booth, V. R. Schild, A. D. Graham, S. N. Olof and H. Bayley, *Sci. Adv.*, 2016, **2**, e1600056.

14 A. Dupin and F. C. Simmel, *Nat. Chem.*, 2019, **11**, 32–39.

15 A. F. Mason, N. A. Yewdall, P. L. W. Welzen, J. Shao, M. van Stevendaal, J. C. M. van Hest, D. S. Williams and L. K. E. A. Abdelmohsen, *ACS Cent. Sci.*, 2019, **5**, 1360–1365.

16 S. Li, X. Wang, W. Mu and X. Han, *Anal. Chem.*, 2019, **91**, 6859–6864.

17 W. Mu, Z. Ji, M. Zhou, J. Wu, Y. Lin and Y. Qiao, *Sci. Adv.*, 2021, **7**, eabf9000.

18 J. Li, Z. Xu, M. Zhu, C. Zhao, X. Wang, H. Chen, X. Liu, L. Wang and X. Huang, *Chem*, 2021, **8**, 784–800.

19 S. Deshpande, F. Brandenburg, A. Lau, M. G. F. Last, W. K. Spoelstra, L. Reese, S. Wunnava, M. Dogterom and C. Dekker, *Nat. Commun.*, 2019, **10**, 1800.

20 V. Percec, D. A. Wilson, P. Leowanawat, C. J. Wilson, A. D. Hughes, M. S. Kaucher, D. A. Hammer, D. H. Levine, A. J. Kim, F. S. Bates, K. P. Davis, T. P. Lodge, M. L. Klein, R. H. DeVane, E. Aqad, B. M. Rosen, A. O. Argintaru, M. J. Sienkowska, K. Rissanen, S. Nummelin and J. Ropponen, *Science*, 2010, **328**, 1009–1014.

21 Y. Miele, Z. Medveczky, G. Holló, B. Tegze, I. Derényi, Z. Hórvölgyi, E. Altamura, I. Lagzi and F. Rossi, *Chem. Sci.*, 2020, **11**, 3228–3235.

22 K. Spustova, E. S. Köksal, A. Ainla and I. Gözen, *Small*, 2021, **17**, 2005320.

23 P. Wen, X. Liu, L. Wang, M. Li, Y. Huang, X. Huang and S. Mann, *Small*, 2017, **13**, 1700467.

24 G. Bolognesi, M. S. Friddin, A. Salehi-Reyhani, N. E. Barlow, N. J. Brooks, O. Ces and Y. Elani, *Nat. Commun.*, 2018, **9**, 1882.

25 Z. Chen, J. Wang, W. Sun, E. Archibong, A. R. Kahkoska, X. Zhang, Y. Lu, F. S. Ligler, J. B. Buse and Z. Gu, *Nat. Chem. Biol.*, 2018, **14**, 86–93.

26 T. Chakraborty, S. M. Bartelt, J. Steinkuhler, R. Dimova and S. V. Wegner, *Chem. Commun.*, 2019, **55**, 9448-9451.

27 T. Chakraborty and S. V. Wegner, *ACS Nano*, 2021, **15**, 9434–9444.

28 A. F. Mason, B. C. Buddingh, D. S. Williams and J. C. M. van Hest, *J. Am. Chem. Soc.*, 2017, **139**, 17309–17312.

29 Y. Qiao, M. Li, D. Qiu and S. Mann, *Angew Chem Int Ed.*, 2019, **58**, 17758–17763.

30 G. Villar, A. J. Heron and H. Bayley, *Nat. Nanotechnol.*, 2011, **6**, 803–808.

31 A. X. Lu, H. Oh, J. L. Terrell, W. E. Bentley and S. R. Raghavan, *Chem. Sci.*, 2017, **8**, 6893–6903.

32 R. J. Peters, M. Marguet, S. Marais, M. W. Fraaije, J. C. van Hest and S. Lecommandoux, *Angew. Chem., Int. Ed.*, 2014, **53**, 146–150.

33 X. Zhang, L. Chen, K. H. Lim, S. Gonuguntla, K. W. Lim, D. Pranantyo, W. P. Yong, W. J. T. Yam, Z. Low, W. J. Teo, H. P. Nien, Q. W. Loh and S. Soh, *Adv. Mater.*, 2019, **31**, 1804540.

34 W. F. Boron, *Adv. Physiol. Educ.* , 2004, **28**, 160–179.

35 X. He, M. Aizenberg, O. Kuksenok, L. D. Zarzar, A. Shastri, A. C. Balazs and J. Aizenberg, *Nature*, 2012, **487**, 214–218.

36 C. Love, J. Steinkühler, D. T. Gonzales, N. Yandrapalli, T. Robinson, R. Dimova and T. D. Tang, *Angew. Chem., Int. Ed.*, 2020, **59**, 5950–5957.

37 P. Gobbo, A. J. Patil, M. Li, R. Harniman, W. H. Briscoe and S. Mann, *Nat. Mater.*, 2018, **17**, 1145–1153.

38 X. Wang, S. Moreno, S. Boye, P. Wen, K. Zhang, P. Formanek, A. Lederer, B. Voit and D. Appelhans, *Chem. Mater.*, 2021, **33**, 6692–6700.

39 N. Martin, J. P. Douliez, Y. Qiao, R. Booth, M. Li and S. Mann, *Nat. Commun.*, 2018, **9**, 3652.

40 C. Wang, A. Fischer, A. Ehrlich, Y. Nahmias and I. Willner, *Chem. Sci.*, 2020, **11**, 4516–4524.

41 L. Heinen, T. Heuser, A. Steinschulte and A. Walther, *Nano Lett.*, 2017, **17**, 4989–4995.

42 Z. Yin, L. Tian, A. J. Patil, M. Li and S. Mann, *Angew. Chem., Int. Ed.*, n/a, e202202302.

43 J. A. Gaitzsch, Dietmar; Wang, Linge; Battaglia, Giuseppe; Voit, Brigitte;, *Angew. Chem., Int. Ed.*, 2012, **51**, 4448–4451.

44 H. Gumz, S. Boye, B. Iyisan, V. Kronert, P. Formanek, B. Voit, A. Lederer and D. Appelhans, *Adv.*

Sci., 2019, **6**, 1801299.

45 S. Moreno, S. Boye, A. Lederer, A. Falanga, S. Galdiero, S. Lecommandoux, B. Voit and D. Appelhans, *Biomacromolecules*, 2020, **21**, 5162–5172.

46 S. Moreno, P. Sharan, J. Engelke, H. Gumz, S. Boye, U. Oertel, P. Wang, S. Banerjee, R. Klajn, B. Voit, A. Lederer and D. Appelhans, *Small*, 2020, **16**, 2002135.

47 X. Wang, S. Moreno, S. Boye, P. Wang, X. Liu, A. Lederer, B. Voit and D. Appelhans, *Adv. Sci.*, 2021, **8**, 2004263.

48 S. Moreno, S. Boye, H. G. A. Ajeilat, S. Michen, S. Tietze, B. Voit, A. Lederer, A. Temme and D. Appelhans, *Macromol. Biosci.*, 2021, **21**, 2100102.

49 B. Iyisan, A. C. Siedel, H. Gumz, M. Yassin, J. Kluge, J. Gaitzsch, P. Formanek, S. Moreno, B. Voit and D. Appelhans, *Macromol. Rapid Commun.*, 2017, **38**, 1700486.

50 G. Liu, J. Tan, J. Cen, G. Zhang, J. Hu and S. Liu, *Nat. Commun.*, 2022, **13**, 585.

51 D. Gräfe, J. Gaitzsch, D. Appelhans and B. Voit, *Nanoscale*, 2014, **6**, 10752–10761.

52 H. Che, S. Cao and J. C. M. van Hest, *J. Am. Chem. Soc.*, 2018, **140**, 5356–5359.

53 A. N. Eremin, I. V. Moroz and R. V. Mikhailova, *Appl. Biochem. Microbiol.*, 2008, **44**, 590–599.

54 H. Kobayashi, M. Ogawa, R. Alford, P. L. Choyke and Y. Urano, *Chem. Rev.*, 2010, **110**, 2620–2640.

55 A. Colom, E. Derivery, S. Soleimanpour, C. Tomba, M. D. Molin, N. Sakai, M. González-Gaitán, S. Matile and A. Roux, *Nat. Chem.*, 2018, **10**, 1118–1125.

56 M. Ali, I. Ahmed, P. Ramirez, S. Nasir, J. Cervera, C. M. Niemeyer and W. Ensinger, *Nanoscale*, 2016, 8, 8583–8590.

57 P. Wen, X. Wang, H. Chen, D. Appelhans, X. Liu, L. Wang and X. Huang, *Chin. J. Chem.*, 2021, **39**, 3386–3392.

58 P. K. Harimech, R. Hartmann, J. Rejman, P. Del Pino, P. Rivera-Gil and W. J. Parak, *J. Mater. Chem. B*, 2015, **3**, 2801–2807.

59 Q. Dai, X. Zhu, S. Abbas, E. Karangwa, X. Zhang, S. Xia, B. Feng and C. Jia, *J. Agric. Food Chem.* , 2015, **63**, 4179–4189.

60 T. Coviello, P. Matricardi, C. Marianecci and F. Alhaique, *J. Controlled Release*, 2007, **119**, 5–24.

61 D. H. Lee, H. J. Sung, D. W. Han, M. S. Lee, G. H. Ryu, M. Aihara, K. Takatori and J. C. Park, *Yonsei Med. J.*, 2005, **46**, 268-274.

62 R. Sjöback, J. Nygren and M. Kubista, Spectrochim. *Acta, Part A*, 1995, **51**, L7–L21.

V. Marshansky and M. Futai, *Curr. Opin. Cell Biol.*, 2008, **20**, 415–426.